

Implicit high-resolution methods for modelling one-dimensional open channel flow

Méthodes implicites à haute résolution pour modéliser l'écoulement unidimensionnel en canaux à surface libre

A. I. DELIS, C. P. SKEELS, and S.C. RYRIE, *Faculty of Computer Studies and Mathematics, University of the West of England, Bristol, BS16 1QY, U.K.*

ABSTRACT

Three implicit high-resolution total variation diminishing (TVD) schemes are presented for solving the Saint-Venant equations. The applicability, performance and validity of these methods are investigated. Recently created benchmark solutions are reproduced for a wide range of cases, which include friction, nonuniform bed slopes, transitions between subcritical and supercritical flow, nonprismatic cross sections and hydraulic jumps. The tests produce satisfactory results without resorting to excessively fine grids. All the methods also produce satisfactory results for an idealized dam-break problem.

RÉSUMÉ

Trois procédés implicites de variation totale décroissante (TVD) à haute résolution sont présentés afin de résoudre les équations de Saint-Venant. Sont examinés l'applicabilité, le fonctionnement et la validité de ces méthodes. Récemment créées, les solutions basées sur les évaluations de performances sont reproduites pour un large choix de cas, incluant friction, déclivités à plateau non uniforme, transition entre flux sous-critique et sur-critiques, coupes non-prismatiques et ruptures hydrauliques. Les tests donnent des résultats satisfaisants sans avoir à recourir à des grilles excessivement fines. Toutes les méthodes donnent aussi des résultats satisfaisants pour un problème de rupture de barrage idéalisée.

1 Introduction

In modern hydraulic engineering practice there is a need for efficient and accurate mathematical simulations which should be able to numerically represent all the physically significant phenomena in a given flow scenario. In this paper, implicit TVD schemes are presented for solving one-dimensional open channel flow hydraulics.

The Saint-Venant hyperbolic equations yield discontinuous solutions in the form of shocks or bores, which can be difficult to represent accurately without the use of a shock-capturing method. Several classical implicit finite difference schemes are commonly used in industry, such as the Pressman scheme, see for example Cunge et al. [2], but they are highly inaccurate in modelling discontinuous flow, and have indiscriminate space-difference approximations in subcritical and supercritical flow regions. It is therefore desirable to develop mathematical/computational models, which are simple to formulate and programme, handle natural channel geometry and deal with discontinuities as accurately as possible. The conservation form of the governing equations is suitable if discontinuities are expected to develop in the solution and to that extent it is essential that the finite difference equivalent be conservatively expressed.

Flux splitting based schemes, like that of the implicit Beam and Warming, [18] were applied by Fennema and Chaudhry [6] to open channel flow problems without source terms and, in general, reported good results, even though quite dissipative. However, these schemes are only first order accurate in space and employ the flux splitting in a nonconservative way. In Jha et al. [10], again the implicit Beam and Warming scheme was used. The continuity equation was evaluated conservatively, but

a nonconservative form of the momentum equation was used. When applied to some cases of dam-break problem, their scheme gave much slower front celerity and higher front height when compared to analytical solutions. Later, Jha et al. [11] proposed a modification for achieving full conservation, employing the use of the Roe-average approximate Jacobian, Roe [15]. This produced a significant improvement in the accuracy of their results.

Total Variation Diminishing (TVD) schemes were introduced by Harten [8] for efficiently solving the Euler equations in gas-dynamics. Their main property is that they are second-order accurate (except at extrema) and oscillation free across discontinuities. Explicit TVD methods applied to the one-dimensional flow equations have been widely reported, see for example Delis and Skeets [5], and they have been proved to be accurate and robust. Variables in a new time level are evaluated at every grid point through simple calculations from already known values. Their main disadvantage lies in the restriction on the time step which is imposed by the Courant-Friedrichs-Lewy (CFL) condition.

To relax the time step restriction, one can consider implicit methods. In this case, the variables are calculated simultaneously at a new time level, through the resolution of a system with as many unknowns as grid points. For non-linear problems, such as the Saint-Venant equations, the resulting system of equations is also non-linear and either a linearisation or an iterative procedure is required. This requires extra computation per time iteration. This is usually compensated by the possibility of achieving unconditional or near unconditional stability for the scheme or allowing the use of very high CFL numbers. The larger the time step we can use, the fewer time steps are

Revision received February, 2000. Open for discussion till April 30, 2001.

required and the more economical the method is in terms of computational time. Implicit TVD schemes have been proved to be unconditionally stable, even when a linearisation technique is applied to solve a non-linear hyperbolic equation, Yee et al. [19]. The present work investigates the more difficult case of implicit schemes modelling channel flow that is represented by a non-linear system of equations. The first attempts along this line of work were presented by Alcrudo et al. [1] employing one form of Yee's [20] symmetric TVD scheme and producing satisfactory results for steady and unsteady open channel problems. The present paper is an extension of the work in Delis and Skeels [4] where two new implicit TVD methods were presented. The first one is based on Harten's [8] modified flux and the second on Van Leer's [17] MUSCL approach. These methods are detailed and extensively tested in the present work, along with Yee's [20] symmetric TVD scheme.

2 Governing Equations

The one-dimensional approach to the unsteady flow of water is governed by the Saint-Venant equations, see Cunge et al. [2] for a derivation. This set of partial differential equations describes a system of hyperbolic conservation laws with source term (\mathbf{G}) and can be written in vector form

$$\frac{\partial \mathbf{U}}{\partial t} + \frac{\partial \mathbf{F}(\mathbf{U})}{\partial x} = \mathbf{G}, \quad (1)$$

where

$$\mathbf{U} = (A, Q)^T, \mathbf{F}(\mathbf{U}) = \left(Q, \frac{Q^2}{A} + gI_1 \right)^T, \\ \mathbf{G} = (0, gI_2 + gA(S_0 - S_f))^T,$$

with A = wetted cross-sectional area; Q = flow rate; g = acceleration due to gravity; S_0 = bed slope; S_f = friction slope. The friction slope S_f is defined in terms of Manning's roughness coefficient n_m , as

$$S_f = \frac{Q^2 n_m^2}{A^2 R^{4/3}}, \quad (2)$$

with $R = A/P$, P being the wetted perimeter. The pressure force integrals I_1, I_2 are calculated in accordance with the geometrical properties of the channel. I_1 represents a hydrostatic pressure force term and I_2 represents the pressure forces due to longitudinal width variations, expressed as

$$I_1 = \int_0^h (h - \eta) b d\eta \quad \text{and} \quad I_2 = \int_0^h (h - \eta) \frac{\partial b}{\partial x} d\eta, \quad (3)$$

where h = water depth; η = integration variable indicating distance from the channel bottom; $b(x, \eta)$ channel width at distance η from the channel bed, expressed as

$$b(x, \eta) = \frac{\partial A(x, \eta)}{\partial \eta}. \quad (4)$$

The Saint-Venant equations are based on the assumptions of hydrostatic pressure distribution and incompressibility of water. The homogeneous part of the system is hyperbolic and responsible for most of the difficulties when it is numerically integrated; namely, the nonlinearity of the flux vector \mathbf{F} may lead to spontaneous discontinuities (jumps) which may have real physical meaning.

The flux vector \mathbf{F} is related to the flow variables \mathbf{U} through the Jacobian \mathbf{J} of \mathbf{F} with respect to \mathbf{U} as

$$\frac{\partial \mathbf{U}}{\partial t} + \mathbf{J} \frac{\partial \mathbf{U}}{\partial x} = 0, \quad (5)$$

and

$$\mathbf{J} = \frac{\partial \mathbf{F}}{\partial \mathbf{U}} = \begin{bmatrix} 0 & 1 \\ gA/b - u^2 & 2u \end{bmatrix}.$$

The hyperbolic nature of the equations ensures that matrix \mathbf{J} has a complete set of independent and real eigenvectors expressed as $\mathbf{e}^{1,2} = (1, u \pm c)^T$, where velocity $u = Q/A$, and celerity $c = \sqrt{gA/b}$. The eigenvalues of \mathbf{J} are given by $a^{1,2} = u \pm c$ and correspond to the two characteristic wavespeeds with their signs providing information about the direction of flow.

3 Approximate Riemann Solver

Previously higher-order modern shock-capturing schemes have been extended from the nonlinear scalar case to one-dimensional nonlinear systems, based on the use of Riemann solvers. In this paper, the discussion and numerical comparisons concentrate on the use of high-resolution TVD schemes with the approximate Riemann solver introduced by Roe [15].

To obtain an approximate solution of equations (1) using a finite difference method, the domain of integration is discretised as (x_i, t_n) , where $x_i = i\Delta x$, $i = 1, 2, \dots$ and $t_n = n\Delta t$, $n = 1, 2, \dots$; Δt is time increment; Δx is grid size in space and suppose that U_i^n is some approximation to $\mathbf{U}(x_i, t_n)$. Godunov [7] was first to develop the idea of advancing the solution to the next time level by solving a set of Riemann problems. The Riemann problem for any system of conservation laws arises if initial data is prescribed as two constant states ($\mathbf{U} = \mathbf{U}_L$ for $x < 0$, $\mathbf{U} = \mathbf{U}_R$ for $x > 0$). Godunov supposed that the initial data could be replaced by piecewise constant set of states for each interface $\{x_{i+\frac{1}{2}}\}$. Thus one can solve the Riemann problem with $\mathbf{U}_L = \mathbf{U}_i$ and $\mathbf{U}_R = \mathbf{U}_{i+1}$, where $\mathbf{U}_i, \mathbf{U}_{i+1}$ denote approximations to \mathbf{U} at the left and right of the cell. This gives an exact solution to the approximate problem assuming that Δt is small enough that the waves from neighbouring interfaces do not interact.

Roe's approximation is based on the assumption that the Jacobian matrix \mathbf{J} of the flux function \mathbf{F} is constant for nonlinear systems in each interval (x_i, x_{i+1}) . It is then a question of constructing an appropriate Jacobian matrix in terms of \mathbf{U}_i and \mathbf{U}_{i+1} in each computational cell so that the shock capturing is automatic.

The approximate Jacobian, $\tilde{\mathbf{J}}$, is defined for the conservative flux splitting following Roe [15], where exact solutions to the following approximate problem were considered:

$$\frac{\partial \mathbf{U}}{\partial t} + \tilde{\mathbf{J}} \frac{\partial \mathbf{U}}{\partial x} = 0. \quad (6)$$

For each computational cell, $\tilde{\mathbf{J}}$ is chosen such that it satisfies the following conditions:

- linear mapping from flow vector \mathbf{U} to flux vector \mathbf{F} is possible,
- $\tilde{\mathbf{J}}_{i+\frac{1}{2}} \Delta_{i+\frac{1}{2}} \mathbf{U} = \Delta_{i+\frac{1}{2}} \mathbf{F}$, where $\tilde{\mathbf{J}}_{i+\frac{1}{2}} = \tilde{\mathbf{J}}(\mathbf{U}_i, \mathbf{U}_{i+1})$,
- $\tilde{\mathbf{J}}(\mathbf{U}, \mathbf{U}) = \mathbf{J}(\mathbf{U}) = \partial \mathbf{F}(\mathbf{U}) / \partial \mathbf{U}$,
- $\tilde{\mathbf{J}}$ has real eigenvalues and a complete set of linearly independent eigenvectors, where the operator $\Delta_{i+\frac{1}{2}}(\bullet) = (\bullet)_{i+1} - (\bullet)_i$.

These conditions for $\tilde{\mathbf{J}}$ ensure conservative properties and consistency with the governing equations. From condition (d) it follows that the eigenvalues $\tilde{a}^{1,2}$ and the eigenvectors $\tilde{\mathbf{e}}^{1,2}$ of $\tilde{\mathbf{J}}$ are of the form

$$\tilde{a}_{i+\frac{1}{2}}^{1,2} = \tilde{u}_{i+\frac{1}{2}} \pm \tilde{c}_{i+\frac{1}{2}} \quad (7)$$

$$\tilde{\mathbf{e}}_{i+\frac{1}{2}}^{1,2} = \left(1, \tilde{a}_{i+\frac{1}{2}}^{1,2} \right)^T, \quad (8)$$

and the problem of finding $\tilde{\mathbf{J}}$ is now transferred to that of finding the average values of \tilde{u} and \tilde{c} that meet the requirements (a)–(d). The following equations for the average velocity and celerity can be obtained (see Delis and Skeels [5] for a derivation)

$$\tilde{u}_{i+\frac{1}{2}} = \frac{Q_{i+1} / \sqrt{A_{i+1}} + Q_i / \sqrt{A_i}}{\sqrt{A_{i+1}} + \sqrt{A_i}}, \quad (9)$$

$$\tilde{c}_{i+\frac{1}{2}}^2 = \begin{cases} g \frac{I_{i+1} - I_i}{A_{i+1} - A_i} & \text{if } A_{i+1} - A_i \neq 0 \\ c_i^2 = g \frac{A_{i+1} + A_i}{B_{i+1} + B_i} & \text{if } A_{i+1} - A_i = 0 \text{ or } \frac{I_{i+1} - I_i}{A_{i+1} - A_i} < 0 \end{cases} \quad (10)$$

Let $\tilde{\mathbf{R}}_{i+\frac{1}{2}}$ denote the right eigenvectors matrix; then since $\tilde{\mathbf{J}}$ has independent and real eigenvectors, its diagonalised form $\text{diag} \left[\tilde{a}_{i+\frac{1}{2}}^k \right]$ can be expressed as

$$\tilde{\mathbf{J}} = \tilde{\mathbf{R}}_{i+\frac{1}{2}} \text{diag} \left[\tilde{a}_{i+\frac{1}{2}}^k \right] \tilde{\mathbf{R}}_{i+\frac{1}{2}}^{-1} \quad k = 1, 2. \quad (11)$$

Condition (d) implies that

$$\Delta_{i+\frac{1}{2}} \mathbf{U} = \sum_{k=1}^2 \alpha_{i+\frac{1}{2}}^k \tilde{\mathbf{e}}_{i+\frac{1}{2}}^k, \quad (12)$$

which means that the jump in states across the k th wave is given by the product of the k th wave strength $\tilde{\alpha}_{i+\frac{1}{2}}^k$ and the appropriate component of the right eigenvector. Thus we find that

$$\alpha_{i+\frac{1}{2}}^{1,2} = \frac{\left[\Delta_{i+\frac{1}{2}} Q + \left(-\tilde{u}_{i+\frac{1}{2}} \pm \tilde{c}_{i+\frac{1}{2}} \right) \Delta_{i+\frac{1}{2}} A \right]}{\pm 2 \tilde{c}_{i+\frac{1}{2}}}. \quad (13)$$

4 Implicit Time Step Iteration

The general form of a one-parameter implicit numerical scheme can be written as

$$\mathbf{U}_i^{n+1} + \lambda \theta \left(\tilde{\mathbf{F}}_{i+\frac{1}{2}}^{n+1} - \tilde{\mathbf{F}}_{i-\frac{1}{2}}^{n+1} \right) - \theta \Delta t \mathbf{G}_i^{n+1} = \mathbf{U}_i^n - \lambda (1 - \theta) \left(\tilde{\mathbf{F}}_{i+\frac{1}{2}}^n - \tilde{\mathbf{F}}_{i-\frac{1}{2}}^n \right) + (1 - \theta) \Delta t \mathbf{G}_i^n \quad (14)$$

where $\lambda = \Delta t / \Delta x$ and $0 \leq \theta \leq 1$, with $\tilde{\mathbf{F}}_{i\pm\frac{1}{2}}^n$ a numerical flux vector; the spatial accuracy of the scheme depends on their form. For $\theta = 0$, the scheme is explicit.

Two other important cases for θ can be identified. For the case where $\theta = \frac{1}{2}$, the time differencing of the scheme corresponds to the trapezium rule. In this case second order accuracy in time can be achieved even for first order numerical fluxes but severe stability restrictions apply. The most important case here is that of $\theta = 1$. This gives the Euler implicit time integration, often called the fully implicit case, since the numerical fluxes are only evaluated at the next time level. It has been proven, see Harten [9] and Yee [19], that for some TVD numerical fluxes the scheme is unconditionally TVD for the non-linear scalar case and that they converge to the physically relevant solution. Thus, the case $\theta = 1$ appears to give the preferable scheme for solving the open channel flow equations.

4.1 Linearised Conservative Implicit (LCI) Form

Solving for \mathbf{U}^{n+1} in [14], we normally need to solve a system of non-linear algebraic equations iteratively. To avoid this costly procedure, the implicit operator is linearised and solved. Following the same procedure as in Yee [20] and Alcrudo et al. [1], a conservative linearised form for (14) is obtained and a linear system has to be solved at each time step.

A family of schemes with the numerical flux vector in (14) written as

$$\tilde{\mathbf{F}}_{i\pm\frac{1}{2}} = \frac{1}{2} \left[\mathbf{F}_i + \mathbf{F}_{i\pm 1} + \tilde{\mathbf{R}}_{i\pm\frac{1}{2}} \Phi_{i\pm\frac{1}{2}} \right], \quad (15)$$

can be derived for different vector functions $\Phi_{i\pm\frac{1}{2}}$. Details of the particular forms of $\Phi_{i\pm\frac{1}{2}}$ are given in the following sections; $\tilde{\mathbf{R}}_{i\pm\frac{1}{2}}$ is calculated from section 3. Following equation (11) we can define a matrix $\mathbf{B}_{i+\frac{1}{2}}$ as

$$\mathbf{B}_{i+\frac{1}{2}} = \tilde{\mathbf{R}}_{i+\frac{1}{2}}^{-1} \text{diag} \left[-\left(\phi_{i+\frac{1}{2}}^k \right) \right] \tilde{\mathbf{R}}_{i+\frac{1}{2}}^{-1}, \quad (16)$$

where $\phi_{i+\frac{1}{2}}^k$ are the elements of $\Phi_{i+\frac{1}{2}}$. Temporarily dropping the subscript indices, \mathbf{B} is calculated as

$$\mathbf{B} = \frac{1}{\tilde{a}^2 - \tilde{a}^1} \begin{bmatrix} \phi^1 \tilde{a}^2 - \phi^2 \tilde{a}^1 & \phi^2 - \phi^1 \\ \tilde{a}^1 \tilde{a}^2 (\phi^2 - \phi^1) & \phi^2 \tilde{a}^2 - \phi^1 \tilde{a}^1 \end{bmatrix}.$$

The numerical fluxes now can be expressed as

$$\tilde{\mathbf{F}}_{i\pm\frac{1}{2}} = \frac{1}{2} \left[\mathbf{F}_i + \mathbf{F}_{i\pm 1} + \mathbf{B}_{i\pm\frac{1}{2}} \Delta_{i\pm\frac{1}{2}} \mathbf{U} \right].$$

In the linearisation introduced, the implicit terms \mathbf{F}^{n+1} and \mathbf{G}^{n+1} are rewritten using a Taylor expansion to give

$$\begin{aligned} \mathbf{F}_i^{n+1} &= \mathbf{F}_i^n + \mathbf{J}_i^n \delta \mathbf{U}_i + O(\Delta t^2) \\ \mathbf{G}_i^{n+1} &= \mathbf{G}_i^n + \mathbf{J}_{\mathbf{G}_i^n} \delta \mathbf{U}_i + O(\Delta t^2), \end{aligned}$$

where $\delta \mathbf{U}_i = \mathbf{U}_i^{n+1} - \mathbf{U}_i^n$ and $\mathbf{J}_{\mathbf{G}}$ is the Jacobian of the term \mathbf{G} with respect to \mathbf{U} . $\mathbf{J}_{\mathbf{G}}$ is expressed in the case of a non-prismatic channel of arbitrary cross-section as

$$\mathbf{J}_{\mathbf{G}} = \frac{\partial \mathbf{G}}{\partial \mathbf{U}} = \begin{bmatrix} 0 & 0 \\ g \left(S_0 + \frac{7}{3} S_f + \frac{\partial B A}{\partial x B^2} \right) & -\frac{2gA}{Q} S_f \end{bmatrix}. \quad (17)$$

The previous linearisation retains a conservative discretization in the implicit part. In addition the following approximation is also made

$$\mathbf{B}_{i+\frac{1}{2}}^{n+1} = \mathbf{B}_{i+\frac{1}{2}}^n.$$

The above simplifications in (14) produce the following block tridiagonal linear system of equations

$$\begin{aligned} \mathbf{A}_1 \delta \mathbf{U}_{i-1} + \mathbf{A}_2 \delta \mathbf{U}_i + \mathbf{A}_3 \delta \mathbf{U}_{i+1} &= -\lambda \left(\tilde{\mathbf{F}}_{i+\frac{1}{2}}^n + \tilde{\mathbf{F}}_{i-\frac{1}{2}}^n \right) + \Delta t \mathbf{G}_i^n \\ i &= 2, \dots, N-1, \end{aligned} \quad (18a)$$

where the \mathbf{A} coefficients are 2×2 matrices with their elements calculated as follows

$$\mathbf{A}_1 = -\frac{\lambda \theta}{2} \left[\mathbf{J}_{i-1} + \mathbf{B}_{i-\frac{1}{2}} \right]^n, \quad (18b)$$

$$\mathbf{A}_2 = \mathbf{I} + \frac{\lambda \theta}{2} \left[\mathbf{B}_{i-\frac{1}{2}} + \mathbf{B}_{i+\frac{1}{2}} \right]^n - \theta \Delta t \mathbf{J}_{\mathbf{G}}, \quad (18c)$$

$$\mathbf{A}_3 = \frac{\lambda \theta}{2} \left[\mathbf{J}_{i+1} - \mathbf{B}_{i+\frac{1}{2}} \right]^n, \quad (18d)$$

with \mathbf{I} being the identity matrix and $\mathbf{J}_{i\pm 1}$ the Jacobian of the physical flux \mathbf{F} evaluated at $i \pm 1$.

The resulting implicit operator is strictly diagonally dominant. Thus, we require only a simple linear systems solver to cheaply solve the linear system. Convergence is defined as when the ‘‘residual’’ (right hand side of equation (18a)) drops to zero or to a predetermined tolerance. The LCI scheme preserves the conservative form of the differencing scheme and is expected to inherit its original properties when a TVD schemes is implemented. Thus it is applicable to steady-state as well as unsteady calculations, without the stability restrictions that usually apply to its explicit counterpart.

4.2 Symmetric LCI Form

This form was presented in Alcrudo et al. [1] where matrix $\mathbf{B}_{i+\frac{1}{2}}$ was calculated based on the flux function of Yee’s [21] symmetric TVD scheme. We define the elements of $\Phi_{i+\frac{1}{2}}$ in equation (15) as

$$\begin{aligned} \left(\phi_{i+\frac{1}{2}}^k \right)^s &= -\psi \left(\tilde{a}_{i+\frac{1}{2}}^k \right) \left[1 - \left(L_{i+\frac{1}{2}}^k / \alpha_{i+\frac{1}{2}}^k \right) \right] \\ k &= 1, 2, \end{aligned} \quad (19)$$

where the function $\psi_{i+\frac{1}{2}}$ is the entropy correction to the eigenvalues $\tilde{a}_{i+\frac{1}{2}}^k$ that guarantees the physically valid discontinuities in the solution. A way to calculate ψ can be found in Delis and Skeels [5].

The function $\psi_{i+\frac{1}{2}}$ is called a limiter function and controls the second order terms, so that a smooth non-oscillatory solution, even in the presence of discontinuities, is guaranteed. In the form of this scheme presented in Alcrudo et al. [1], the arguments of the limiter function were calculated in an upwind fashion. Here we have to modify this approach in order to be consistent with Yee’s original approach of the symmetric scheme. Thus the limiting function can be one of the following, having as arguments the wave strengths calculated in section 3,

$$L_{i+\frac{1}{2}}^k = m \left(\alpha_{i-\frac{1}{2}}^k, \alpha_{i+\frac{1}{2}}^k, \alpha_{i+\frac{3}{2}}^k \right), \quad (20a)$$

$$L_{i+\frac{1}{2}}^k = m \left[2\alpha_{i-\frac{1}{2}}^k, 2\alpha_{i+\frac{1}{2}}^k, 2\alpha_{i+\frac{3}{2}}^k, \frac{1}{2} \left(\alpha_{i-\frac{1}{2}}^k + \alpha_{i+\frac{3}{2}}^k \right) \right], \quad (20b)$$

$$L_{i+\frac{1}{2}}^k = \frac{\left| \alpha_{i-\frac{1}{2}}^k \alpha_{i+\frac{1}{2}}^k \right| + \left| \alpha_{i+\frac{1}{2}}^k \alpha_{i+\frac{3}{2}}^k \right| + \alpha_{i-\frac{1}{2}}^k \alpha_{i+\frac{1}{2}}^k + \alpha_{i+\frac{1}{2}}^k \alpha_{i+\frac{3}{2}}^k}{2 \left| \alpha_{i+\frac{1}{2}}^k \right| + \left| \alpha_{i-\frac{1}{2}}^k \right| + \left| \alpha_{i+\frac{3}{2}}^k \right|}, \quad (20c)$$

$$\begin{aligned} L_{i+\frac{1}{2}}^k &= \max \left[0, \min \left(2\alpha_{i+\frac{1}{2}}^k, \alpha_{i-\frac{1}{2}}^k, \alpha_{i+\frac{3}{2}}^k \right), \right. \\ &\quad \left. \min \left(\alpha_{i+\frac{1}{2}}^k, 2\alpha_{i-\frac{1}{2}}^k, 2\alpha_{i+\frac{3}{2}}^k \right) \right], \end{aligned} \quad (20d)$$

where the limiting function $m(a, b)$ is the minmod limiter function defined as

$$m(a, b) = \text{sgn}(a) \max[0, \min(|a|, \text{sgn}(a)b)].$$

The limiters (20a)-(20d) will be referred as the L_m , L_c , L_{vl} and L_{sb} respectively.

The LCI form with the implicit operator on the left-hand side is first order accurate if one simply sets the limiter functions to be zero when calculating $\mathbf{B}_{i+\frac{1}{2}}$ in equations (18b)–(18d). This form has been found to be more stable in practice, admitting higher CFL numbers.

In Delis and Skeels [4], two methods previously used in gas-dynamics, namely the modified flux and the MUSCL schemes, were combined with the above linearised implicit form and used to solve the Saint-Venant equations. These methods are presented and detailed in the next two sections.

4.3 Modified Flux LCI Form

The second-order modified flux approach, was originally developed by Harten [8]. Yee [20] produced a modification less diffusive and easier to implement than Harten's. Here Yee's modified version will be described. The elements of $\Phi_{i+\frac{1}{2}}$ in (15) are now given by

$$\begin{aligned} (\phi_{i+\frac{1}{2}}^k)^{mf} &= \mu(\tilde{\alpha}_{i+\frac{1}{2}}^k) \frac{(L_{i+1}^k + L_i^k)}{\alpha_{i+\frac{1}{2}}^k} - \psi(\tilde{\alpha}_{i+\frac{1}{2}}^k + \gamma_{i+\frac{1}{2}}^k), \\ k &= 1, 2. \end{aligned} \quad (21a)$$

where now the function μ is defined as

$$\mu(a) = \frac{1}{2} \psi(a) + \lambda \left(\theta - \frac{1}{2} \right) a^2, \quad (21b)$$

for time-dependent calculations and

$$\mu(a) = \frac{1}{2} \psi(a), \quad (21c)$$

for steady calculations. The γ function, is defined as

$$\gamma_{i+\frac{1}{2}}^k = \mu(\tilde{\alpha}_{i+\frac{1}{2}}^k) \begin{cases} (\Delta_{i+\frac{1}{2}} L) / \alpha_{i+\frac{1}{2}}^k & \alpha_{i+\frac{1}{2}}^k \neq 0 \\ 0 & \alpha_{i+\frac{1}{2}}^k = 0 \end{cases}. \quad (21d)$$

The limiter function L_i^k can be one of the following forms

$$L_i^k = m(\alpha_{i-\frac{1}{2}}^k, \alpha_{i+\frac{1}{2}}^k), \quad (21e)$$

$$L_i^k = \frac{(\alpha_{i+\frac{1}{2}}^k \alpha_{i-\frac{1}{2}}^k + |\alpha_{i+\frac{1}{2}}^k \alpha_{i-\frac{1}{2}}^k|)}{(\alpha_{i+\frac{1}{2}}^k + \alpha_{i-\frac{1}{2}}^k)}, \quad (21f)$$

$$L_i^k = m \left[2\alpha_{i-\frac{1}{2}}^k, 2\alpha_{i+\frac{1}{2}}^k, \frac{1}{2}(\alpha_{i+\frac{1}{2}}^k + \alpha_{i-\frac{1}{2}}^k) \right], \quad (21g)$$

$$L_i^k = \max \left[0, \min \left(2\alpha_{i+\frac{1}{2}}^k, \alpha_{i-\frac{1}{2}}^k \right), \min \left(\alpha_{i+\frac{1}{2}}^k, 2\alpha_{i-\frac{1}{2}}^k \right) \right]. \quad (21h)$$

We will refer to the limiters (21e)–(21h) as the L_M , L_{VL} , L_C and L_{SB} respectively.

Using (21b), the scheme is second order accurate in space and time regardless of θ . However, with this scheme a steady state solution depends on the time step. Using (21c) makes the scheme second order in space, but first order in time if $\theta = 1$ and ensures that the steady state solution does not depend on the time step Δt . Second order accuracy in space and time can be achieved for (21c), if $\theta = \frac{1}{2}$ is chosen, at the cost of more restrictive stability limits.

Using the modified flux approach, scheme (14) has proven in Harten [9] to be unconditionally TVD for $\theta = 1$ in the non-linear scalar case. In practice, unconditional stability arising from linear stability analysis rarely carries over to non-linear system cases with discontinuous solutions. However, the main interest is a less restrictive time-step bound than the one for the explicit methods, combined with high-order accuracy.

Using the modified flux approach, the matrix $\mathbf{B}_{i+\frac{1}{2}}$ corresponding to (21a) is given by

$$\mathbf{B}_{i+\frac{1}{2}} = \tilde{\mathbf{R}}_{i+\frac{1}{2}} \text{diag} \left[-(\phi_{i+\frac{1}{2}}^k)^{mf} \right] \tilde{\mathbf{R}}_{i+\frac{1}{2}}^{-1} \quad k = 1, 2. \quad (22a)$$

The LCI form with the implicit operator on the left-hand side is first order accurate if one simply sets the limiter function to be zero, and the scheme will still then be in conservation form.

4.4 MUSCL LCI Form

The MUSCL-TVD interpolation formula, introduced by Van Leer [17], provides a one parameter family of second-order schemes and one third-order scheme. TVD properties are guaranteed for the geometric approach using a slope rather than flux limiter which limits the gradients of the dependent variables. The MUSCL scheme replaces the arguments, \mathbf{U}_i and \mathbf{U}_{i+1} , of the numerical fluxes by $\mathbf{U}_{i+\frac{1}{2}}^L$ and $\mathbf{U}_{i+\frac{1}{2}}^R$, where $\mathbf{U}_{i+\frac{1}{2}}^L$ and $\mathbf{U}_{i+\frac{1}{2}}^R$ are calculated as follows

$$\mathbf{U}_{i+\frac{1}{2}}^L = \mathbf{U}_i + \frac{1}{4} \left[(1-m) \Delta_{i-\frac{1}{2}}^+ + (1+m) \Delta_{i+\frac{1}{2}}^+ \right], \quad (23)$$

$$\mathbf{U}_{i+\frac{1}{2}}^R = \mathbf{U}_{i+1} - \frac{1}{4} \left[(1-m)\Delta_{i+\frac{3}{2}}^+ + (1+m)\Delta_{i+\frac{1}{2}}^+ \right], \quad (24)$$

where

$$\Delta_{i+\frac{1}{2}}^- = m \left(\Delta_{i+\frac{1}{2}} \mathbf{U}, \beta \Delta_{i-\frac{1}{2}} \mathbf{U} \right), \quad (25)$$

$$\Delta_{i+\frac{1}{2}}^+ = m \left(\Delta_{i+\frac{1}{2}} \mathbf{U}, \beta \Delta_{i+\frac{3}{2}} \mathbf{U} \right), \quad (26)$$

where β is a compression parameter whose value is in the range

$$1 \leq \beta \leq \frac{3-m}{1-m}, \quad m \neq 1.$$

The spatial order of accuracy is determined by the chosen value of m . In this study $m = 1/3$ is used, giving third-order accuracy in space.

Using the MUSCL approach with the LCI form it is possible to achieve third order accuracy in space. Since the limiting process in the MUSCL reconstruction takes place in the variables' slopes, before being introduced to the numerical fluxes, this approach is more straightforward to use when producing the corresponding LCI form. Now the $\mathbf{B}_{i+\frac{1}{2}}$ has the simple form

$$\mathbf{B}_{i+\frac{1}{2}} = \hat{\mathbf{R}}_{i+\frac{1}{2}} \text{diag} \left[\psi \left(\hat{a}_{i+\frac{1}{2}}^k \right) \right] \hat{\mathbf{R}}_{i+\frac{1}{2}}^{-1} \quad k = 1, 2. \quad (27)$$

since

$$\hat{\phi}_{i+\frac{1}{2}}^k = -\psi \left(\hat{a}_{i+\frac{1}{2}}^k \right) \hat{a}_{i+\frac{1}{2}}^k \quad k = 1, 2. \quad (28)$$

In equations (27) and (28), $\hat{a}_{i+\frac{1}{2}}^k$ and $a_{i+\frac{1}{2}}^k$ are simply calculated as in section 3, but the arguments \mathbf{U}_i and \mathbf{U}_{i+1} have been replaced by $\mathbf{U}_{i+\frac{1}{2}}^L$ and $\mathbf{U}_{i+\frac{1}{2}}^R$ respectively.

5 Numerical Results

The main interest here is to test if the LCI TVD schemes can offer a larger time step bound with high accuracy. Here, steady-state problems with known exact solutions are solved using the three implicit TVD methods. The results for each approach are compared with each other and the analytical solutions. The idealized dam-break problem was also chosen as a classical example of unsteady flow, with shocks, to test accuracy. All tests were performed with $\theta = 1$ and a first order implicit operator.

5.1 Steady Test Problems with Analytical Solutions

The problems solved here are from MacDonald et al. [13, 14] and MacDonald [12], where benchmark test problems with analytical solutions have been constructed for the full Saint-Venant equations. The type of flow for each problem is determined by varia-

ble bed slope S_0 , which is given as a function of the exact water depth and its derivative, see Appendix for details. In this section, the unsteady computational models presented are compared in their predictions of steady state solutions. The test problems include extreme cases with hydraulic jumps and multiple, smooth or not, transitions. The existence of analytical solutions for these test problems enables the calculation of a definite measure of the performance of the LCI methods described.

Problem 1 [Super-Subcritical Flow with Hydraulic Jump] A 1000m long rectangular channel of width $B = 10\text{m}$ has Manning's roughness coefficient $n_m = 0.02$. The flow is supercritical at inflow, changes via a hydraulic jump to subcritical halfway along the channel, and remains subcritical thereafter.

Problem 2 [Super-Sub-Supercritical Flow with Hydraulic Jump] A rectangular channel 100m long has width $B = 10\text{m}$ and $n_m = 0.03$. The flow is supercritical at inflow, changing via a hydraulic jump to subcritical at $x = 100/3\text{m}$ and smoothly changing again to supercritical for the last third of the channel.

Problem 3 [Sub-Super-Subcritical Flow with Hydraulic Jump] A 1000m long trapezoidal channel has $B = 10 + 2h$, $P = 10 + 2h\sqrt{2}$ and $n_m = 0.02$. The flow is subcritical at inflow, changes smoothly to supercritical at $x = 300\text{m}$, and then returns to subcritical, via a hydraulic jump, at $x = 600\text{m}$.

Problem 4 [Subcritical Flow] A 5000m long trapezoidal channel ($B = 10 + 4h$, $P = 10 + 2h\sqrt{5}$) and has $n_m = 0.03$. The flow is subcritical at inflow and remains subcritical throughout the channel.

Problem 5 [Super-Subcritical with Hydraulic Jump] The channel for this problems is non-uniform rectangular with variable channel width given by

$$B(x) = 10 - 5 \exp \left(-10 \left(\frac{x}{200} - \frac{1}{2} \right)^2 \right). \quad (29)$$

The width profile is illustrated in figure 1. A 200m long rectangular channel, with width given by equation (29), has $n_m = 0.03$. The flow is supercritical at inflow and changes to subcritical, via a hydraulic jump, $x = 120\text{m}$,

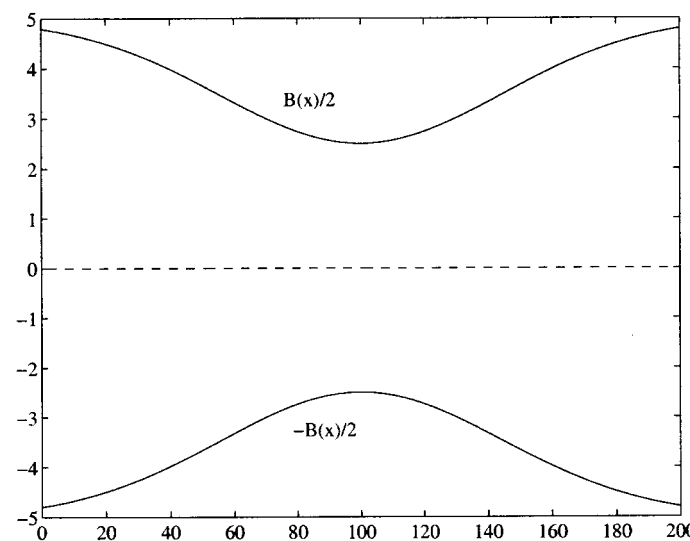


Fig. 1. Channel width for problem 5.

All the test problems previously described have a constant discharge of $20 \text{ m}^3\text{s}^{-1}$. For those test problems for which the outflow is subcritical, the downstream boundary condition is that water depth is a pre-determined constant; the value of the constant is that given by the exact solution itself.

In figures 2 and 3, the depth and discharge numerical solutions for the three implicit schemes are compared for problem 1. A 51 point space discretisation was used and the results presented are for a CFL number of 30 for all schemes. The numerical depth profiles follow closely the exact solution for all methods. The L_m limiter for the symmetric scheme and the L_C for the modified produced the most accurate results. Away from the jump, the discharge fields are constant for all methods with the MUSCL ($\beta=1$) scheme being the most accurate.

In figure 3, and in some of the subsequent figures, it is evident that there is some loss of continuity near the hydraulic jump itself. This is probably a consequence of numerical diffusion, arising from the property of TVD schemes that their accuracy at extrema is first order rather than second order. The test cases studied also show the difficulty of retaining the conservation property when the source term is included.

In figure 4, the total variation evolution for the three methods is presented plotted in logarithmic scale for every time step. The total variation definition, in m^2 , for a vector grid function for the system case is calculated as

$$TV(\mathbf{U}) = \sum_i \sum_{k=1}^2 \left| \alpha_{i+\frac{1}{2}}^k \right|. \quad (30)$$

All the methods retain the basic TVD property after the first three steps, with the total variation diminishing until the steady-state is reached.

In figure 5, the convergence history is plotted on a logarithmic scale. Convergence is defined as occurring when the “residual” (right handside of equation (18a), measured in units of metres) drops to zero or to a predetermined tolerance. Convergence was achieved in 25 steps for the MUSCL scheme, 27 for the symmetric scheme and 28 for the modified flux. An explicit TVD scheme ($\theta = 0$) running with a CFL number of 0.95 converges much slower and requires about 800 steps for convergence to the same accuracy. Although the computational cost per time step is much cheaper for an explicit scheme, the overall computational cost for these implicit method is 60% cheaper by that of an explicit methods for the same problem and with the same number of grid points use. It was observed that convergence could not be achieved for CFL numbers greater than 30 for the symmetric LCI scheme.

For problem 2, the results are shown in figures 6 and 7. All schemes use a 51 point discretisation and a CFL number of 30. The symmetric scheme (L_{sb} limiter) is much more diffusive in the supercritical region of the flow before the jump and deviates from the constant discharge state during the same region. The MUSCL ($\beta = 2$) and modified flux (L_C limiter) produce more accurate numerical solutions for both depth and discharge. All the schemes correctly predict the jump. The only difference

observed between these two accurate schemes is that the MUSCL scheme converged in 43 time steps and the modified flux in 63.

Next, problem 3 with the trapezoidal channel was tested. For a 51 point grid, a CFL number of 40 was used. Results are shown in figures 8 and 9. Again all the methods follow closely the solution representing accurately all flow regimes, including the smooth transition from subcritical to supercritical flow at $x = 300\text{m}$. The jump is correctly predicted with the MUSCL ($\beta = 4$) and the modified flux (L_C limiter), while the symmetric scheme (L_{vj} limiter) undershoots the jump at the grid point immediately before. In the discharge profiles, the symmetric scheme is the most inaccurate near the jump with severe oscillations.

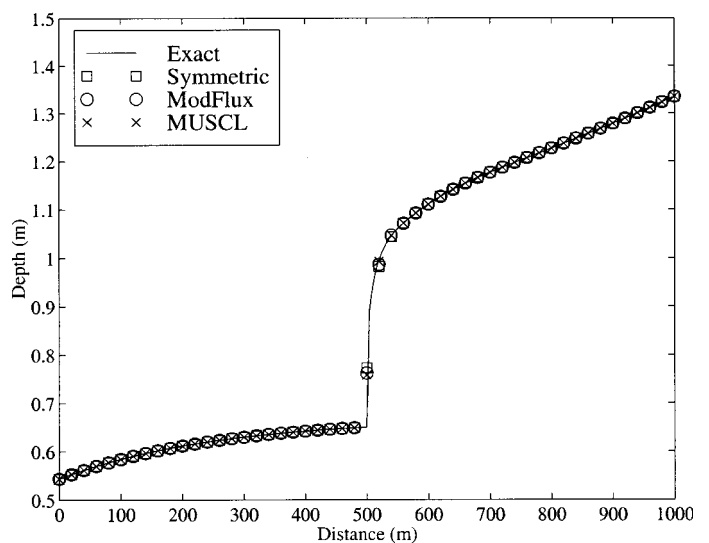


Fig. 2. Comparison of the three LCI TVD schemes for problem 1.

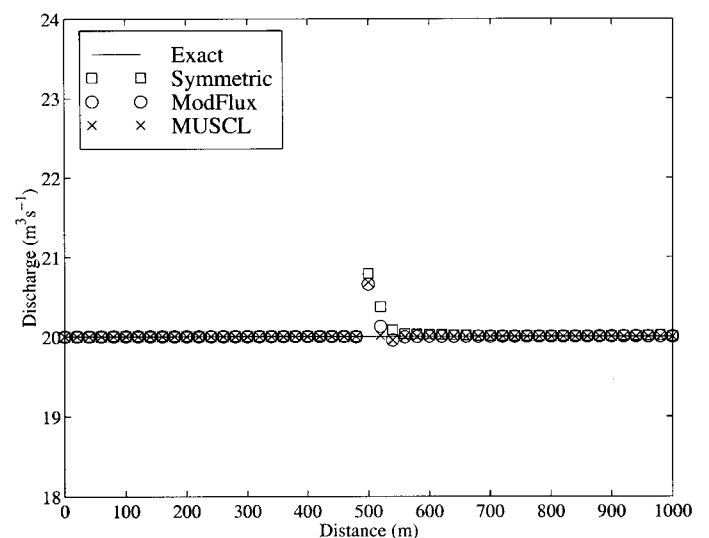


Fig. 3. Discharge fields for the three LCI TVD schemes for problem 1.

The total variation evolution, displayed in figure 10 for the three implicit schemes, shows that all methods retain the basic TVD property for a trapezoidal channel and a high CFL number

after the first four or five time steps. The convergence history is shown in figure 11, where all the schemes converge in a slightly oscillatory manner, but in few time steps.

The next test problem is problem 4 (totally subcritical flow in a trapezoidal channel). This problem rigorously tests the conservation properties of the numerical schemes. For this problem the symmetric scheme failed to converge for CFL numbers greater than 5. The residual decreased and then became trapped in some limited cycle. This effect is called “residual plateauing” and is common in steady calculations when using schemes with non-linear limiters. Hence, no results are presented here for this scheme. The limit for achieving convergence with the modified flux (L_C limiter) was a CFL number of 30. The results for the MUSCL ($\beta = 4$) scheme were produced with a CFL number of 40. As shown in figure 12, the results for the numerical depth for both methods are almost identical and are close to the exact solution. In the discharge field, see figure 13, the numerical results are slightly above the correct level for both schemes, but in almost constant state. For both schemes, the percentage mass flow error was found to be below 1% throughout the channel.

The total variation evolution diminishes for both implicit schemes as shown in figure 14. The MUSCL scheme converged after 72 time steps and the modified flux after 82 steps. With the same spatial grid approximation, an explicit scheme running with CFL number between 0.6–0.9, required between 2000–3000 time steps for convergence. Thus, these implicit schemes have the potential to provide substantial savings in computational time.

Next results for problem 5 with a non-prismatic channel are presented. Again, the symmetric scheme appeared not to converge for CFL numbers greater than one. This was checked for all limiters and different spatial discretisations. The other schemes were run with a CFL number of 40 and a spatial grid of 41 points. Results for the MUSCL ($\beta = 2$) and modified flux (L_{VL} limiter) schemes are shown in figures 15–16. Some numerical diffusion on the supercritical part of the flow and incorrect jump position by one grid point can be observed. The two schemes produced almost identical depth profiles. In the discharge predictions, the MUSCL scheme is close to the exact solution in the supercritical region of the flow before the jump, and the modified flux is closer to the exact solution in the subcritical region after the jump. In general the modified flux required more iterations to converge than the MUSCL scheme, as can be seen in figure 17. The modified flux exhibited some problems at the final stages before convergence.

In general the implicit TVD methods require more CPU time (typically about three times more) per time step than explicit TVD methods, but result in an enhanced convergence rate, thereby reducing the total CPU time required to achieve convergence. The number of time steps for convergence monotonically decreases as the CFL number increases. However, the reduction in the number of steps was found to be less pronounced for a CFL number above 40. This was the case for all the test problems presented here.

The accuracy of the solutions presented was measured in terms of the l_1 norm and are shown in Table 1. This provides a quan-

titative measure of a method’s performance, although qualitative measures tend to be more popular. Both approaches provide complementary means of determining the solutions quality (when the exact solution is available).

Table 1. The l_1 errors for the three LCI TVD methods.

Test Problem Number	LCI Method					
	Symmetric		ModFlux		MUSCL	
	Depth	Discharge	Depth	Discharge	Depth	Discharge
1	2.90D-03	3.13D-02	2.54D-03	1.80D-02	2.20D-03	1.48D-02
2	3.02D-03	3.89D-02	1.65D-03	1.22D-02	1.27D-03	2.80D-03
3	4.41D-03	4.96D-02	3.04D-03	2.86D-02	2.73D-03	2.97D-02
4	-	-	2.82D-03	1.07D-01	3.11D-03	1.06D-01
5	-	-	2.29D-02	2.56D-02	2.27D-02	2.51D-02

5.2 Idealised Dam-Break Problem

We consider a wide ($B = 10\text{m}$), frictionless channel with flat-bottom surface. The dam is initially located at the middle of the 2,000m long rectangular channel. The water depth ratio is h_d/h_u where h_u is the upstream depth and h_d is the downstream depth. The governing equations are given by (1) with $\mathbf{G} = 0$. The dam collapses at $t = 0$ and the resulting flow consists of a shock wave (bore) travelling downstream and a rarefaction wave (depression wave) travelling upstream. The upstream depth h_u was kept constant at 10m, while the downstream depth was different for each problem. When the depth ratio is greater than 0.5, the flow throughout the channel remains subcritical. For depth ratios smaller than 0.5, the flow downstream is supercritical while remaining subcritical upstream. For very small values of the ratio h_d/h_u the flow regime becomes strongly supercritical downstream and the shock wave can be difficult to capture. The analytical (exact) solutions for these sample problems were calculated using Stoker’s [16] method and shown as a solid line in the all the figures.

The implicit schemes presented here were derived for solving steady-state problems with strong discontinuities in gas-dynamics. Nevertheless, here they are tested for the unsteady calculation of idealised dam-break-problems. In river flow, discontinuities are generally weaker. The proposed LCI TVD models the problem with a depth ratio of 0.05. The tests presented here are for a 101 grid point spatial discretisation. The depth profiles along the channel are again calculated at time 50s.

In figures 18(a)–18(d), the results of the MUSCL scheme use a depth ratio of 0.05 and four different CFL numbers. Similarly, we present the results for the symmetric scheme in figures 19(a)–19(d) and for the modified flux in figures 20(a)–20(d). All schemes produced accurate profiles for CFL numbers up to one. The MUSCL scheme with $\beta = 4$ produced better shock resolution, as displayed in figure 18(a), while the modified flux (L_{VL} limiter) was more accurate in the rarefaction wave prediction, as shown in figure 19(a). All three methods reached the 50s limit after almost the same number of time step iterations. For higher CFL numbers, the numerical solutions become more diffusive, especially in the prediction of the rarefaction wave, see figures 18(d), 19(d) and 20(d), but they still predict the general features of the exact solution. To ensure stability, the value of the compression parameter for the MUSCL has to

decrease as the CFL value increases and the modified flux limiter is changed to the L_C limiter. The L_C limiter gave the most accurate results for the symmetric scheme. Results for the lower depth ratio of 0.005 for the three LCI TVD methods and for different CFL numbers can be found in Delis [3].

As was mentioned earlier, second order accuracy in time can be achieved. The implicit models can be improved to second order accuracy in time using $\theta = 1/2$ in equation (14) and following that in equation (18a). However, this choice severely restricts the TVD stability limits. The LCI models are no longer TVD for CFL values greater than 2, as proved in Yee [19]. Results for this option applied to the idealised dam-break problem can be found in Delis [3]. The same problem was observed for the symmetric and MUSCL LCI schemes. This verifies the theoretical constraints given by Yee [19]. For the symmetric scheme the restriction is more severe, with the CFL restricted to less than $4/3$, see Yee [21].

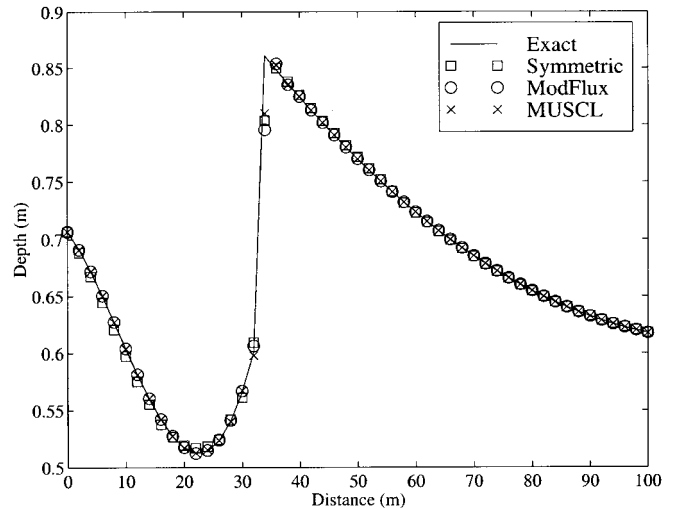


Fig. 6. Comparison of the three LCI TVD schemes for problem 2.

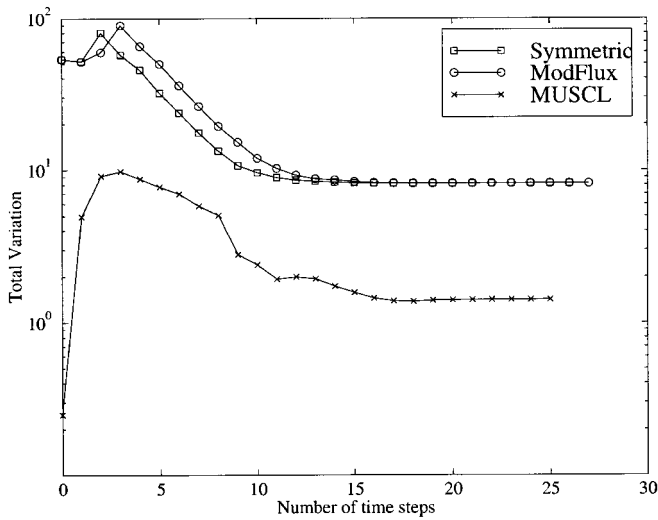


Fig. 4. Total Variation evolution for the three LCI TVD schemes for problem 1.

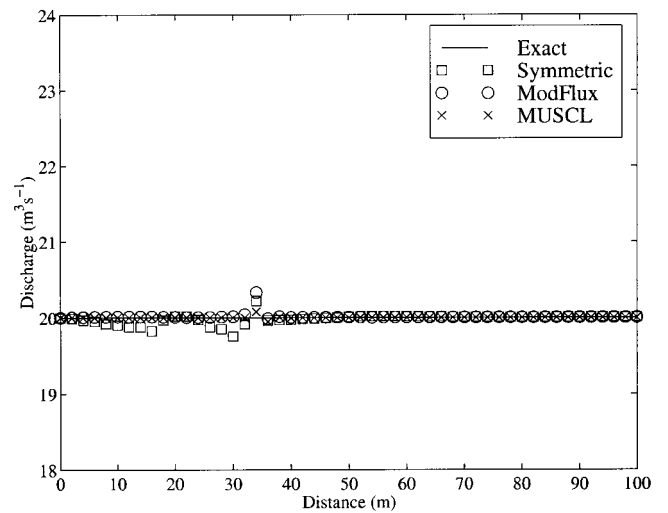


Fig. 7. Discharge fields for the three LCI TVD schemes for problem 2.

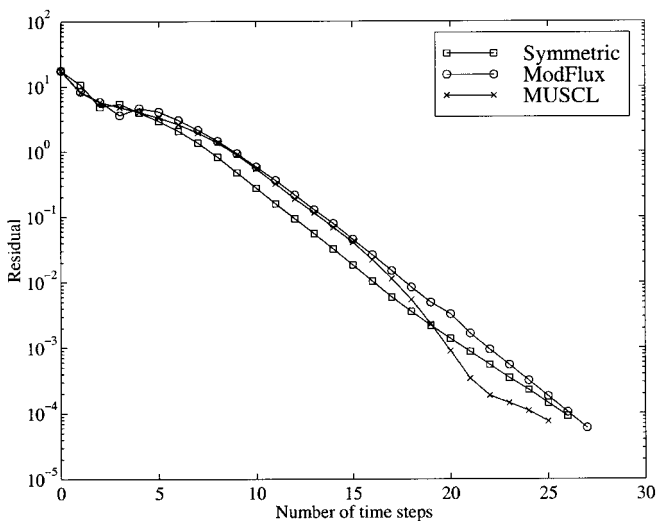


Fig. 5. Convergence history for the three LCI TVD schemes for problem 1.

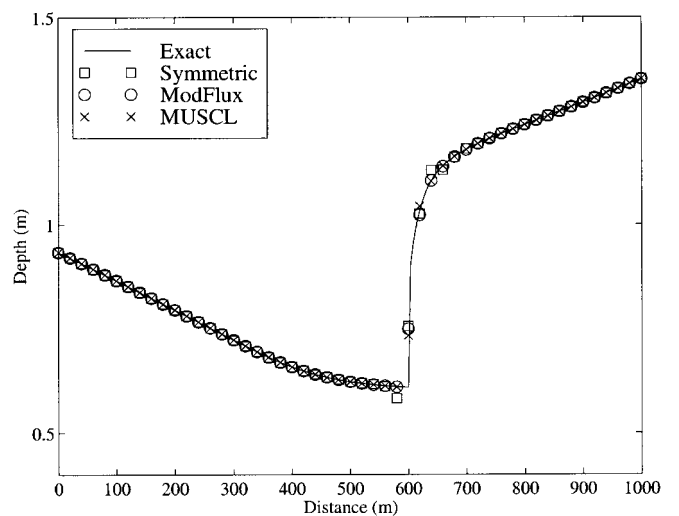


Fig. 8. Comparison of the three LCI TVD schemes for problem 3.

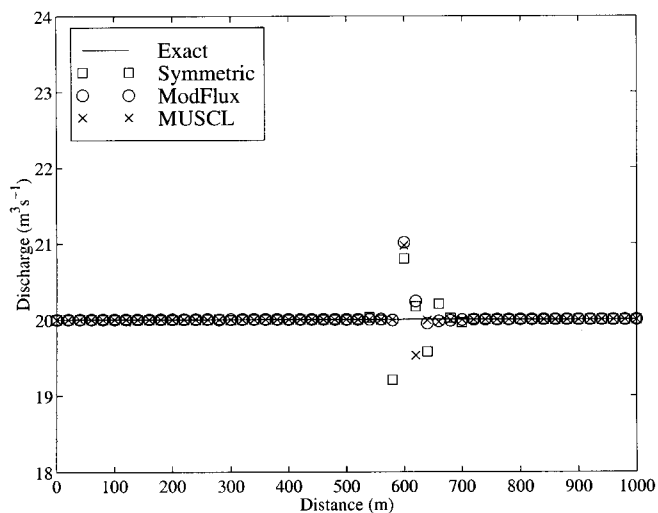


Fig. 9. Discharge fields for the three LCI TVD schemes for problem 3.

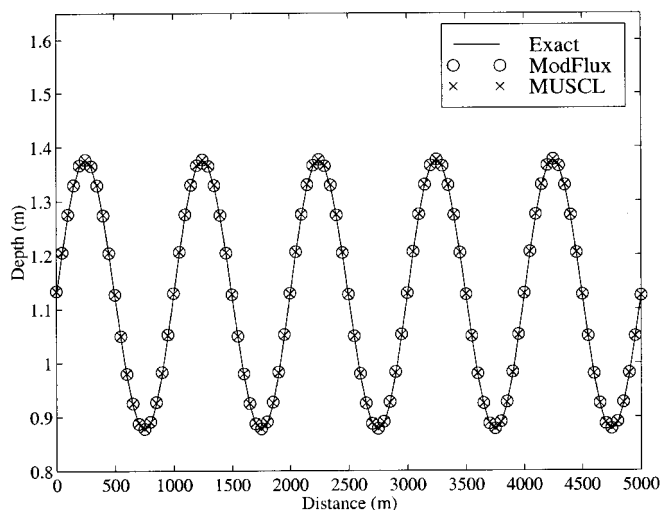


Fig. 12. Comparison for two LCI TVD schemes for problem 4.

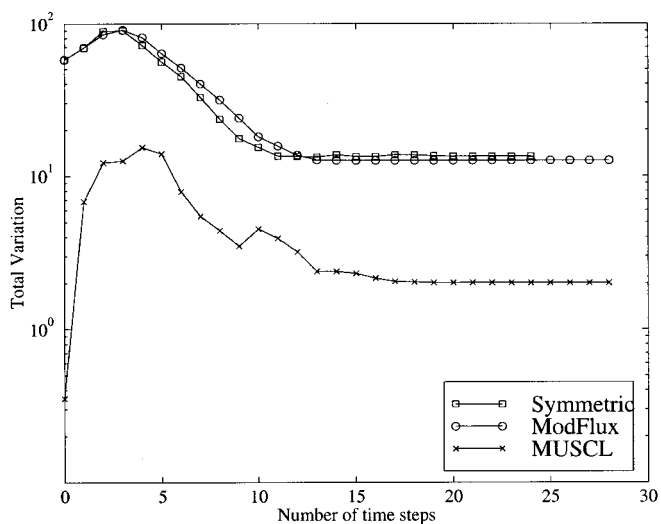


Fig. 10. Total Variation evolution for the three LCI TVD for problem 3.

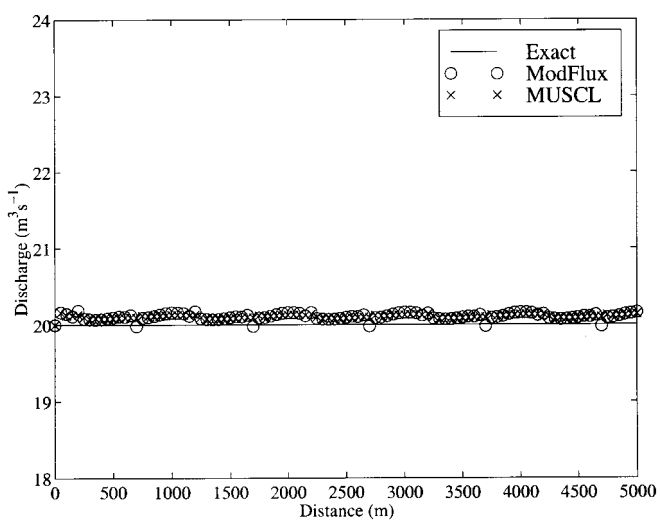


Fig. 13. Discharge fields for two LCI TVD schemes for problem 4.

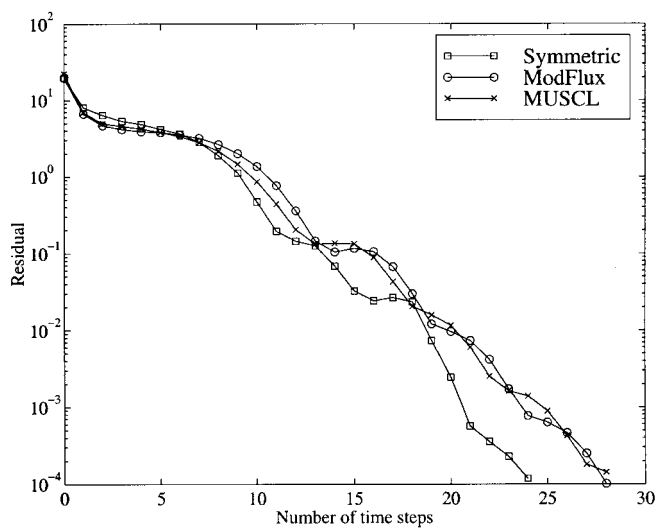


Fig. 11. Convergence history for the three LCI TVD schemes for problem 3.

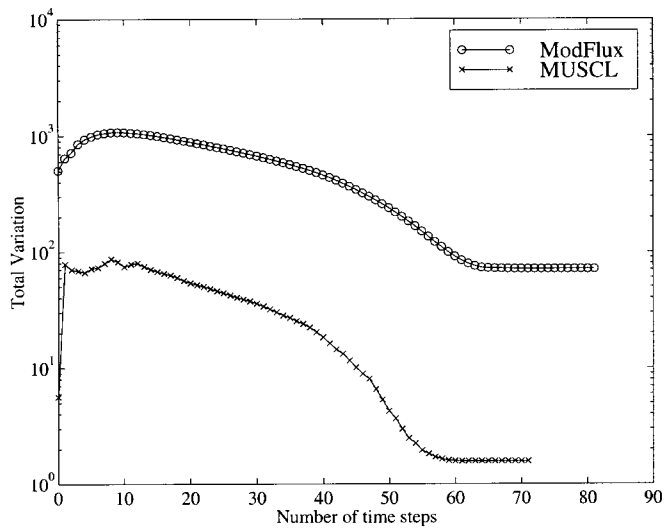


Fig. 14. Total Variation evolution for two LCI TVD schemes for problem 4.

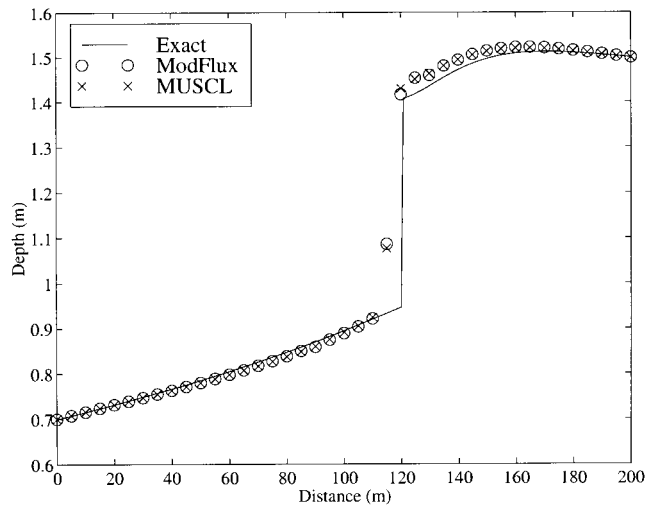


Fig. 15. Comparison of two LCI TVD schemes for problem 5.

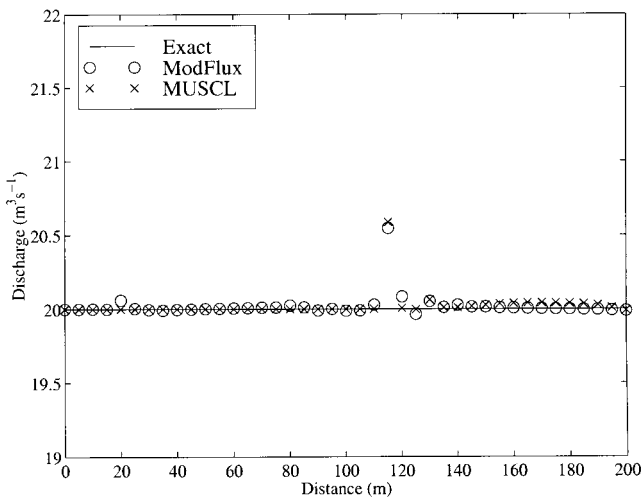


Fig. 16. Discharge fields of two LCI TVD schemes for problem 5.

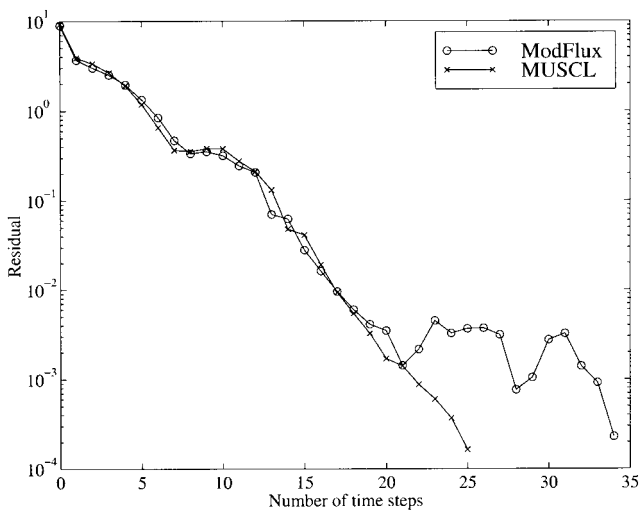


Fig. 17. Residual for two LCI TVD schemes for problem 5.

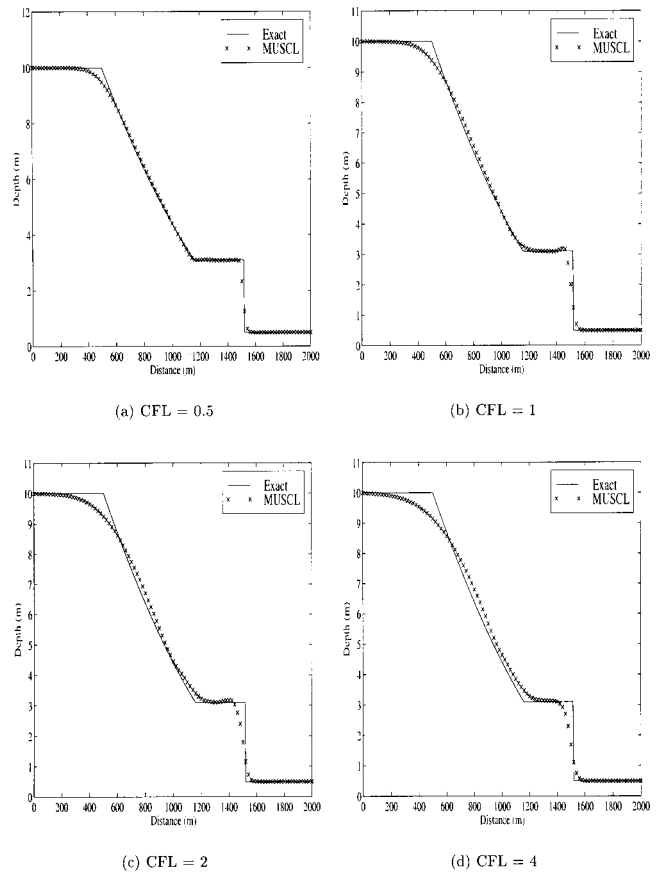


Fig. 18. LCI MUSCL scheme for the idealized dam-break problem; Depth Ratio = 0.05.

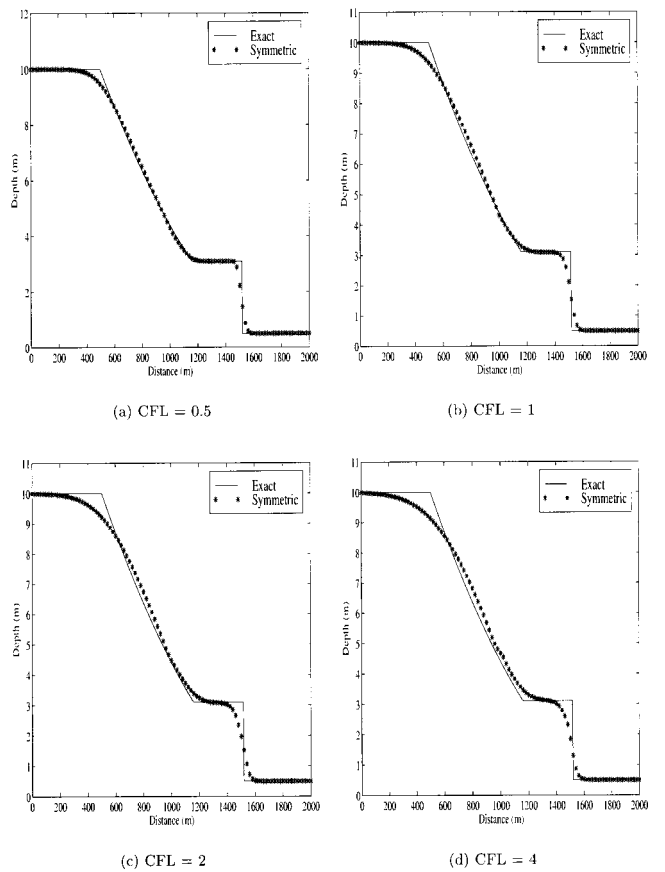


Fig. 19. LCI Symmetric scheme for the idealized dam-break problem; Depth Ratio = 0.05.

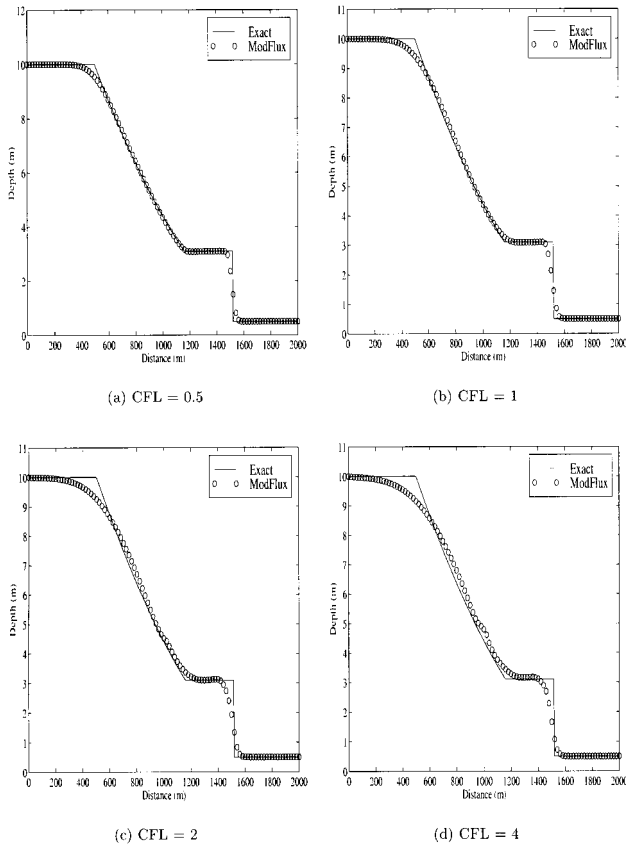


Fig. 20. LCI Modified Flux scheme for the idealized dam-break problem; Depth Ratio = 0.05.

6 Conclusions

In this paper, three conservative implicit TVD methods, suitable for solving the Saint-Venant equations, have been presented and detailed. The linearised versions of the symmetric, modified flux and MUSCL TVD methods were tested for a wide range of steady problems. Various limiter functions were presented and tested. All steady and unsteady problems were solved without resorting to excessively fine grids.

The modified flux and MUSCL methods were able to cope well with all the steady cases of subcritical and mixed regime flows with strong discontinuities. They provided accurate results without being restricted by the usual CFL stability condition. The symmetric approach failed to converge when strong subcritical flow was imposed and for non-uniform channel geometry. The MUSCL method was proven to be the most efficient and robust in all the steady cases allowing high CFL values in all the test performed. The methods retained the TVD property for very high CFL numbers, and diverse channel geometries. The implicit schemes converged in few time step iterations, compared to explicit schemes, with potentially significant savings in computational cost. This is advantageous for the calculation of steady solutions. These are required as initial data for unsteady simulations. Good conservation of mass was also observed with low percentage of mass flow error.

All the proposed models were also able to handle the unsteady dam-break problem. They remained stable and relatively accu-

rate provided that the CFL number is not overly large for $\theta = 1$. For the small number of grid points used, the computational time is not excessive. Further work should investigate adapting the fully implicit schemes so they become second order accurate in time.

Notations

A	cross-sectional area of flow;
$\mathbf{A}_{1,2,3}$	coefficient matrices;
a	eigenvalues of \mathbf{J} ;
B	free-surface width;
$b(\eta)$	channel width at distance η from channel bed;
c	celerity;
\mathbf{e}	matrix of eigenvectors;
\mathbf{F}	flux vector;
$\tilde{\mathbf{F}}$	numerical flux vector;
\mathbf{G}	matrix containing source terms;
g	acceleration due to gravity;
h	water depth;
I_1, I_2	pressure force integrals;
i	grid location in space;
\mathbf{J}	Jacobian of \mathbf{F} with respect to \mathbf{U} ;
\mathbf{J}_G	Jacobian of \mathbf{G} with respect to \mathbf{U} ;
$\tilde{\mathbf{J}}$	approximated Jacobian;
k	integer index;
L	limiter function;
N	total number of grid points;
n	time index;
n_m	Manning's roughness coefficient;
P	wetted perimeter;
Q	discharge;
\mathbf{R}	right eigenvector matrix of \mathbf{J} ;
S_f	friction slope;
S_0	bed slope;
u	flow velocity;
\mathbf{U}	flow variables vector;
α	wave strength;
Δ	space difference operator;
δ	time difference operator;
η	integration variable indicating distance from channel bed;
θ	time weighting parameter ;
Φ	numerical dissipation vector;
ϕ	element of Φ ;
ψ	entropy fix function;
\sim	denotes averaged variables for the approximate Jacobian.

References

1. F. ALCRUDO, P. GARCIA-NAVARRO, and A. PRIESTLEY. An implicit method for water flow modelling in channels and pipes. *J. Hydraulic Res.*, 32:721, 1994.
2. J. A. CUNGE, F. M. HOLLY, and A. VERWAY. *Practical Aspects of Computational River Hydraulics*. Pitman Publishing Ltd., London, 1980.
3. A. I. DELIS. Implicit high-resolution schemes for modelling open channel flows. Research and Consultancy Report No. 19, Univer-

sity of the West of England, Department of Mathematical Sciences, 1998.

4. A. I. DELIS and C. P. SKEELS. Implicit TVD methods for modeling discontinuous channel flows. In J. S. Gulliver, editor, Energy and water: Sustainable development (Proceedings of theme D: the XXVII Congress of the International Association for Hydraulic Research), page 222. ASCE, New York, 1997.
5. A. I. DELIS and C. P. SKEELS. TVD schemes for open channel flow. *Int. J. Numer. Meth. Fluids*, 26(7):791, 1998.
6. R. J. FENNEMA and H. M. CHAUDHRY. Simulation of one-dimensional dam-break flows. *J. of Hydraulic Res.*, 25(1):41, 1987.
7. S. K. GODUNOV. Finite difference method for numerical computation of discontinuous solutions of the equations of fluid dynamics. *Mathematicheskii Sbornik*, 47(3):271–306, 1959.
8. A. HARTEN. High resolution schemes for hyperbolic conservation laws. *J. Comp. Phys.*, 49:357, 1983.
9. A. HARTEN. On a class of high resolution total-variation-stable finite difference schemes. *SIAM Journal of Numerical Analysis*, 21:1, 1984.
10. A. JHA, J. AKIYAMA, and M. URA. Modelling unsteady open channel flows. (Modification to Beam and Warming scheme). *J. of Hydraulic Engineering*, 120(4):461, 1994.
11. A. JHA, J. AKIYAMA, and M. URA. A fully conservative Beam and Warming scheme for transient open channel flow. *J. of Hydraulic Res.*, 34(5):605, 1996.
12. I. MACDONALD. Analysis and computation of steady open channel flow. PhD thesis, University of Reading, 1996.
13. I. MACDONALD, M. J. BAINES, N. K. NICHOLS, and P. K. SAMUELS. Comparison of some steady state Saint-Venant solvers for some test problems with analytical solutions. Numerical Analysis Report 2/95, University of Reading, Department of Mathematics, 1995.
14. I. MACDONALD, M. J. BAINES, N. K. NICHOLS, and P. K. SAMUELS. Analytic benchmark solutions for open channel flows. *J. of Hydraulic Engineering*, 123(11):1041, 1997.
15. P. L. ROE. Approximate Riemann solvers, parameter vectors, and difference schemes. *J. Comp. Phys.*, 43:357–372, 1981.
16. J. J. STOKER. *Water Waves*. Interscience Publishers, Inc., New York, 1986.
17. B. VAN LEER. Towards the ultimate conservative difference scheme. V. A second order sequel to Godunov's method. *J. Comp. Phys.*, 32:101, 1979.
18. R. F. WARMING and R. M. BEAM. An implicit finite difference algorithm for hyperbolic systems in conservation law form. *J. Comp. Phys.*, 22:87, 1976.
19. H. C. YEE. Linearised form of implicit TVD schemes for the multidimensional Euler and Navier-Stokes equations. *Comp. and Maths, with Appls*, 12A(4/5):413, 1986.
20. H. C. YEE. Construction of explicit and implicit symmetric TVD schemes and their applications. *J. Comp. Phys.*, 68:151, 1987.
21. H. C. YEE. A class of high resolution explicit and implicit shock-capturing methods. NASA TM-101088, 1989.

Appendix

The slopes and analytical solutions for the test problems 1–5 in section 5.1 are given here following MacDonald et al. [13, 14] and MacDonald [12].

A.1 Test Problem 1

The slopes of the channel for this problem is given by

$$S_0(x) = \left[1 - \frac{4}{gh(x)^3}\right]h'(x) + 0.16 \frac{[2h(x) + 10]^{4/3}}{[10h(x)]^{10/3}},$$

where

$$h(x) = \begin{cases} \left(\frac{4}{g}\right)^{1/3} \left[\frac{9}{10} - \frac{1}{6} \exp\left(\frac{-x}{250}\right) \right] & 0 \leq x \leq 500 \\ \left(\frac{4}{g}\right)^{1/3} \left\{ 1 + \sum_{k=1}^3 a_k \exp\left[-20k\left(\frac{x}{1000} - \frac{1}{2}\right)\right] \right\} + \frac{4}{5} \exp\left(\frac{x}{1000} - 1\right) & 500 < x, 1000, \end{cases}$$

with $a_1 = -0.348427$, $a_2 = 0.552264$ and $a_3 = -0.555580$. The flow is supercritical at inflow with depth $h(0)$ and subcritical at outflow with depth $h(1000)$. The solution to this problem is given by the $h(x)$ function.

A.2 Test Problem 2

The slope of the channel is given by

$$S_0(x) = \left[1 - \frac{4}{gh(x)^3}\right]h'(x) + \frac{9}{2500h(x)^2} \left(\frac{1}{5} + \frac{1}{h(x)}\right)^{4/3},$$

where

$$h(x) = \begin{cases} \left(\frac{4}{g}\right)^{1/3} \left[-10.7872 \left(\frac{x}{100} - \frac{1}{3}\right)^4 + 18.8777 \left(\frac{x}{100} - \frac{1}{3}\right)^3 + 17.9329 \left(\frac{x}{100} - \frac{1}{3}\right)^2 + 3.1725 \left(\frac{x}{100} - \frac{1}{3}\right) + 0.850042 \right] & x \leq \frac{100}{3} \\ \left(\frac{4}{g}\right)^{1/3} \left[\frac{5}{6} + \frac{(100-x)}{200} + \frac{4}{10} \left(\frac{x}{100} - \frac{1}{3}\right) \left(\frac{x}{100} - 1\right) \right] & x > \frac{100}{3} \end{cases}$$

The flow is supercritical at inflow and outflow. Hence, the boundary conditions are inflow discharge of $20\text{m}^3\text{s}^{-1}$ and $h(0)$. The exact depth for this problem is given by $h(x)$.

A.3 Test Problem 3

For this problem the slope of the channel is given by

$$S_0(x) = \left\{ 1 - \frac{400[10 + 2h(x)]}{g[10 + h(x)]^3 h(x)^3} \right\} h'(x) + 0.16 \frac{[10 + 2h(x)\sqrt{2}]^{4/3}}{[10 + h(x)]^{10/3} h(x)^{10/3}}$$

where

$$h(x) = \begin{cases} 0.723449 \left[1 - \tanh\left(\frac{x}{1000} - \frac{3}{10}\right) \right] & 0 \leq x \leq 300 \\ 0.723449 \left\{ 1 - \frac{1}{6} \tanh\left[6\left(\frac{x}{1000} - \frac{3}{10}\right)\right] \right\} & 300 < x \leq 600 \\ \frac{3}{4} + \sum_{k=1}^3 a_k \exp\left[-20k\left(\frac{x}{1000} - \frac{3}{5}\right)\right] + \frac{3}{5} \exp\left(\frac{x}{1000} - 1\right) & 600 < x \leq 1000 \end{cases}$$

with $a_1 = -0.111051$, $a_2 = 0.026876$ and $a_3 = -0.217567$. The flow is subcritical at inflow and outflow. Hence, the boundary conditions are inflow discharge of $20\text{m}^3\text{s}^{-1}$ and outflow depth $h(100)$. The exact depth for this problem is given by $h(x)$.

A.4 Test Problem 4

The bed slope for this problem is

$$S_0(x) = \left\{ 1 - \frac{400[10 + 4h(x)]}{g[10 + h(x)]^3 h(x)^3} \right\} h'(x) + 0.36 \frac{[10 + 2h(x)\sqrt{5}]^{4/3}}{[10 + 2h(x)]^{10/3} h(x)^{10/3}}$$

where

$$h(x) = \frac{9}{8} + \frac{1}{4} \sin\left(\frac{\pi x}{500}\right).$$

The flow is subcritical at inflow and outflow with outflow depth $h(5000)$. The depth solution to this problem is given by the $h(x)$ function.

A.5 Test Problem 5

The channel with $B(x)$ is given by equation (29) and the bed slope is given by

$$S_0(x) = \left\{ 1 - \frac{400B(x)}{9.08665h(x)^3 B(x)^3} \right\} h'(x) + \frac{144[B(x) + 2h(x)]^{4/3}}{h(x)^{10/3} B(x)^{10/3}} - \frac{400B'(x)}{9.08665h(x)^2 B(x)^3}$$

where

$$h(x) = 0.7 + 0.3 \left[\exp\left(\frac{x}{200}\right) - 1 \right],$$

for $x \leq 120\text{m}$, and for the remainder of the reach is of the form

$$h(x) = \exp[-0.1(x - 120)] \sum_{k=0}^2 a_k \left(\frac{x - 120}{80}\right)^k + 1.5 \exp\left[-0.1\left(\frac{x}{200} - 1\right)\right],$$

where $a_0 = -0.154375$, $a_1 = 0.108189$ and $a_2 = -2.014310$. The flow is supercritical at inflow with depth $h(0)$ and subcritical at outflow with depth $h(200)$. The solution to this problem is given by the $h(x)$ function.